HHS Public Access

Author manuscript

Int J Radiat Oncol Biol Phys. Author manuscript; available in PMC 2021 August 01.

Published in final edited form as:

Int J Radiat Oncol Biol Phys. 2021 February 01; 109(2): 603–613. doi:10.1016/j.ijrobp.2020.09.046.

High Resolution pO_2 Imaging Improves Quantification of the Hypoxic Fraction in Tumors during Radiotherapy

Xu Cao[1,2], **Srinivasa Rao Allu**[3,4], **Shudong Jiang**[1,5], **Jason R. Gunn**[1], **Cuiping Yao**[1,6], **Xin Jing**[1,6], **Petr Bruza**[1], **David J. Gladstone**[1,5,7], **Lesley A. Jarvis**[5,7], **Jie Tian**[2,8], **Harold M. Swartz**[9], **Sergei A. Vinogradov**[3,4], **Brian W. Pogue**[1,5,*]

[1]Dartmouth College, Thayer School of Engineering, Hanover, New Hampshire, USA

[2]Xidian University, Engineering Research Center of Molecular & Neuroimaging, Ministry of Education, School of Life Science and Technology, Xi'an, Shaanxi, China

[3]Department of Biochemistry and Biophysics, Perelman School of Medicine, University of Pennsylvania, Philadelphia, PA, USA.

[4]Department of Chemistry, School or Arts and Sciences, University of Pennsylvania, Philadelphia, PA, USA.

[5]Norris Cotton Cancer Center, Dartmouth-Hitchcock Medical Center, Lebanon, NH, USA.

[6]Xi'an Jiaotong University, Institute of Biomedical Analytical Technology and Instrumentation, School of Life Science and Technology, Key Laboratory of Biomedical Information Engineering of Ministry of Education, Xi'an, Shaanxi, China

[7]Department of Medicine, Geisel School of Medicine, Dartmouth College, Hanover, New Hampshire, USA.

[8]CAS Key Laboratory of Molecular Imaging, Institute of Automation, Chinese Academy of Sciences, Beijing, China.

[9]Department of Radiology, Geisel School of Medicine, Dartmouth College, Hanover, New Hampshire, USA.

Abstract

Hypoxia exists extensively in solid tumors and is thought to be an important factor in radiation resistance, leading to failures in radiotherapeutic local control. The ability to non-invasively image

[*]**Corresponding Author:** Brian W. Pogue, Ph. D, Thayer School of Engineering at Dartmouth, Phone: (603) 646-3861; brian.w.pogue@dartmouth.edu.

Author Contributions

X.C. designed experiments, analyzed data and wrote the paper. X.C., J.R.G., C.Y., and X.J. carried out the experiments and edited the manuscript. S.J., H.M.S. and P.B. provided advice on experimental design and data analysis and edited the manuscript. D.J.G., and L.A.J. advised on radiotherapy design and data interpretation and edited the manuscript. J.T. edited the manuscript. S.R.A. synthesized the probe Oxyphor PtG4. S.A.V. performed photophysical measurements, oxygen calibrations, provided partial support of the work and edited the manuscript. B.W.P. conceived the study, analyzed the data, provided full support of the work and edited the manuscript.

Competing financial interests

B.W.P. is a founder and president of DoseOptics LLC, which develops camera systems and software for radiotherapy imaging of Cherenkov light for dosimetry. S.A.V. has partial ownership of Oxygen Enterprises Ltd, which owns the intellectual property for dendritic phosphorescent oxygen probes technology (US Pat. No. 9,556,213; US, 2017/0137449 A1). All other authors declare no competing interests.

tumor oxygen levels would be highly instrumental for clinical radiotherapy planning and adaptation, especially in cases of chronic or transient regional hypoxia. However, the extreme microscopic heterogeneity of tumors makes it difficult to characterize tumor hypoxia based on imaging because there is no tool for high spatial resolution imaging of oxygen in humans. Here, subcutaneous xenograft tumor pO2 maps were imaged at submillimeter spatial resolution by Cherenkov excited luminescence imaging (CELI) *in vivo* during radiotherapy. In transitioning from voxel sizes of 200 μm to 3mm, the median pO_2 values increased by a few mmHg, while the hypoxic fraction decreased by more than 50%. When looking at radiation responsive tumors, the median pO_2 changes were just a few mmHg for before versus after treatment, while the hypoxic fraction changed by 50%, but this latter change could only be seen at the higher spatial resolution sampling. This study supports the hypothesis that for adequate measurements of the tumor response to radiation therapy, oxygen imaging with high spatial resolution is required in order to accurately characterize the hypoxic fraction. Median pO_2 or similar surrogate quantities obtained from low resolution measurements are commonly used today in clinical practice, however these parameters are much less sensitive to changes in the tumor microenvironment than the tumor hypoxic fraction obtained from high-resolution oxygen images.

Keywords

Hypoxia; Cherenkov; pO_2; lifetime; time-gated

Classification:

Biological Sciences

Introduction

Hypoxia is an important factor in radiotherapy of many solid tumors. This observation is because oxygen is thought to acutely enhance radiobiologic damage through oxygen-fixation of DNA damage during therapy, and also hypoxia presence can mediate molecular signaling mechanisms for cellular adaptation and resistance (1–3). Patients with hypoxic tumors commonly exhibit poor outcomes across a range of tumor genotypes and phenotypes (4–6). The most common clinical prescription to tumors with known hypoxia is to boost the radiation dose (7–10). Although this and other strategies have been attempted to overcome tumor resistance, there is still a challenge to accurately quantify the scope of hypoxia within tumors. This challenge comes from the fact that tumors are composed of extreme spatial variations in oxygenation between capillaries and regions of the solid mass, on the scale of microns. These variations are largely to highly heterogeneous capillary perfusion across the irregular neovascular networks serving the growing tumor tissue, and oxygen diffusion distance limitations to the tumor cells. The inability to evaluate this known heterogeneity of oxygenation in tumors has been limited due the lack of methods for non-invasive, fast and repeatable mapping of pO_2 distributions in tumor tissues (11, 12). In this study, the technique based on phosphorescence quenching imaging of pO_2 in vivo has been applied to tumors during radiotherapy to evaluate the spatial sensitivity to different measures of tumor hypoxia and evaluate how they relate to radiation responsiveness.

Methods of tissue oxygenation sampling, such as in vivo by microelectrodes or ex vivo by tissue immunohistochemical hypoxia markers, in principle are capable of high spatial resolution, but these techniques suffer from being inherently invasive. In addition, both methods have limited ability to sample the entire tumor volume, which reduces their clinical value (13, 14). Non-invasive macroscopic imaging methods have become more commonly used to image human tumor oxygenation, especially Positron Emission Tomography (PET) with either fluoromisonidazole (FMISO) (15, 16) or fluoroazomycin arabinoside (FAZA) (17–19). Both these tracers are being evaluated to optimize radiotherapy delivery (20–22). However, there are fundamental limits to PET spatial resolution and complex relationships between the signals by these tracers and the actual tissue oxygenation (23, 24). While preclinical PET studies with these compounds have submillimeter resolutions, these observations may not translate into the whole-body PET imaging in clinical radiotherapy, which has much lower spatial resolution because of the high degree of heterogeneity of oxygen (25). Indeed, the factor that affects radiation therapy the most is the *hypoxic fraction of a tumor*, which is defined as the fractional volume of cells that is below 10mmHg, and therefore has lower oxygen enhancement ratio effect. Much of the definitive work on the definition of hypoxia and OER has been demonstrated in vitro, and perhaps some of the most useful in vivo data to support this has been shown in Eppendorf electrode data (26). However, to date there is no established methodology to fully characterize the hypoxic fraction of human tumors, and imaging tools that sample at lower resolution tend to skew this parameter significantly (Fig. 1A) by averaging over larger areas to provide a volume-weighted mean or median value. Overall, today there is no macroscopic imaging method that could provide information on tumor oxygenation with adequate spatial resolution and accuracy to inform therapeutic radiation delivery.

Imaging of pO_2 in tumors is possible using the combination of Cherenkov-Excited Luminescence Imaging (CELI) and the phosphorescence quenching method(27, 28) using excitation light generated within tissues during radiation therapy (29–31). Oxyphor PtG4 (32, 33) is phosphorescent probe (SI Appendix, Fig. S1), that can be used with CELI to directly image tumor pO_2 distributions at the time of radiation delivery (34–37). As with most optical imaging modalities, the acquired lateral spatial resolution of pO_2 images is determined by the lens design and the tissue optics. With appropriate commercial camera lenses, CELI imaging can resolve spatial maps at 200 microns lateral voxel diameter, which makes it possible to assess tumor hypoxia at sub-millimeter spatial resolution at millimeters depth below the surface of tumors. In this study, Cherenkov-pO_2 imaging was used to quantify tumor hypoxia in two types of mouse xenograft tumors (Fig. 1B). Both a radiation responsive and a radiation resistant tumor line were treated with hypofractionated MegaVolt (MV) X-ray irradiation to determine how imaging of tumor oxygenation is correlated with radiation response. Sub-millimeter spatial resolution oxygen distributions could then be compared to millimeter-level spatial images to investigate the influence of imaging spatial resolution on the quantification of tumor hypoxia parameters and how they correlate with response metrics.

Results

Hypoxia assessment based on immunohistochemical staining

While there are limitations to immunocytochemical staining with pimonidazole as an indirect hypoxia marker, it provides a method to obtain oxygen distributions in tumors with perhaps the highest possible spatial resolution. The efficacy of staining with pimonidazole was first verified under conditions with comparative control studies without pimonidazole or the antibody (SI Appendix, Fig. S2A). CD31 staining was also used to observe the vascularity patterns relative to spatially co-registered tumor hypoxia staining with pimonidazole (SI Appendix, Fig. S2B). Pimonidazole staining showed high heterogeneity both in a single section of a tumor and at different depths within a tumor (Fig. 2A). To investigate the influence of resolution on the hypoxic quantification, the spatial resolution was varied by smoothing the pimonidazole staining images with different smoothing filters (SI Appendix, Fig. S3). For a pimonidazole section, the original resolution (0.5 μm) was reduced to 0.01~5 mm after the smoothing process, and the hypoxic areas shrank gradually with this resolution change (Fig. 2B). The hypoxic fraction of a representative tumor section decreased monotonously with resolution, and the value for 3 mm resolution image (correlating to that approximately used in PET imaging) was reduced to about half of that for 0.01 mm resolution image (correlating to single cell level spatial resolution) (Fig. 2C). The heterogeneity of the tumor oxygenation led to a variety of hypoxic fractions at different depths for the same tumor (Fig. 2C). While there was no difference in hypoxic fractions for sections measured with 0.01 mm resolution and 0.2 mm resolution, measurements with 3 mm resolution gave a significantly decreased hypoxic fraction (Fig. 2D). The hypoxic fraction averaged across the whole tumor also showed similar trend (Fig. 2E). The analysis that excluded known areas of necrosis showed no change in the tendency to quantify the hypoxic fractions at different resolutions (SI Appendix, Fig. S4).

Hypoxia assessment based on CELI

Four CELI images (Fig. 3A) were acquired with different delay times during the radiotherapy, 24 h after IV administration of Oxyphor PtG4 (200 μL of 200 μM solution). After single-exponential fitting, the pO_2 images (Fig. 3B) were estimated using the Stern-Volmer equation using calibration constants obtained in the independent measurements (32). The ability to image pO_2 *in vivo* with CELI was first verified by imaging a muscle with high oxygen content and a tumor with low oxygen content after local injection of Oxyphor PtG4 (SI Appendix, Fig. S5). The resolution of the original pO_2 image was 0.2 mm, and all the other pO_2 images were smoothed with different smoothing filters. Hypoxic maps (Fig. 3C) were obtained by dividing pO_2 images into hypoxic (pO2<10 mmHg) and normoxic (pO2≥10 mmHg) regions. The hypoxic fractions in the images were lower when the images were obtained at lower resolution. The pO2 histograms with lower resolution show that the distributions concentrated towards higher values (Fig. 3D)The median pO_2 values of the whole tumor were slightly higher, and no statistically significant differences were observed between the median pO_2 values obtained with 0.2mm and other lower resolutions (Fig. 3E). The hypoxic fraction of the whole tumor decreased as a monotonic function of resolution, and a statistically significant difference was observed between hypoxic fractions for 0.2mm

resolution and 2mm ~ 5mm (Fig. 3F). The differences in the hypoxic fraction values were more significant than the differences between the median pO_2 values.

pO_2 imaging of FaDu and MD-MBA-231 tumors

Two groups of mice with subcutaneous MDA-MB-231 or FaDu tumors were imaged by CELI after IV injection of Oxyphor PtG4 to demonstrate the oxygenation differences between the different tumor lines. The tumors were subjected to 25 Gy radiation doses using a 6MV X-ray beam with 5 Gy/fraction daily for 5 days, and CELI was performed during the treatment on the first and last days to investigate pO_2 changes of the two tumor lines after radiotherapy. Hypoxic areas in the MDA-MB-231 tumor on the first day was smaller than those on the fifth day, while there was no obvious decrease in the FaDu tumor (Fig. 4A). The pO_2 histogram shifted to a higher value from the first day to the fifth day for MDA-MB-231 tumor, but no such change occurred for the FaDu tumors. Hypoxic areas reduced significantly in both tumor lines when the resolution was reduced to 3 mm (Fig. 4B). The distribution of pO_2 histograms showed a narrower range for 3 mm resolution, as compared to 0.2 mm resolution. The radiotherapy significantly increased median pO_2 values in the MDA-MB-23 tumor more than in the FaDu tumor for both 0.2 mm and 3 mm resolutions (Fig. 4C). Additionally, in the case of 0.2 mm resolution, the hypoxic fractions in the MDA-MB-23 tumor on the 5^{th} day showed lower values relative to the 1^{st} day, but the FaDu tumor did not show a significance difference (Fig. 4D). While the difference of hypoxic fraction in MDA-MB-23 tumors between the 1^{st} and 5^{th} day was negligible when the resolution was reduced to 3mm. More detailed results are provided in SI Appendix, Fig. S6.

Outcome and pO_2 imaging for single dose radiotherapy

To demonstrate the correlation between pO_2 parameters and response to radiotherapy, a cohort of 10 mice with subcutaneous MDA-MB-231 were imaged with CELI during treatment. The pO_2 images were obtained during a single fraction of radiotherapy, using an 8 Gy radiation dose (SI Appendix, Fig. S7A). The assay of response followed mouse tumor volumes daily until they increased by 3X relative to the day of treatment. Mice were divided to a low-responding group (4 mice) and high-responding group (6 mice) for analysis (SI Appendix, Fig. S7B and C).

Although the tumors were the same tumor line, the low-response group showed more pO_2 values less than 10 mmHg and thus a larger hypoxic fraction as compared to the high-response tumors (Fig. 5A). After reducing the spatial resolution to 3mm, the pO_2 images for all the tumors changed and the small hypoxic regions disappeared. The range of pO_2 histograms was squeezed from 0 ~ 30 mmHg for 0.2mm spatial resolution, to 10 ~ 20 mmHg for 3mm spatial resolution. The smoothness in the low spatial resolution pO_2 image removed almost the pO_2 values lower than 10 mmHg and higher than 20 mmHg. The median pO_2 values for high-response tumors were significantly higher than low-response tumors with 0.2mm spatial resolution, but no difference was seen with 3mm spatial resolution (Fig. 5B). The median pO_2 values increased for all the tumors from high to low spatial resolution, but only the high-response tumors showed a significant difference. Similarly, the hypoxic fractions for high-response tumors were significantly lower than low-response tumors with a spatial resolution of 0.2mm, but no difference with 3mm spatial

resolution. The central observation was that spatial resolution significantly decreased the observed hypoxic fraction (Fig. 5C). As defined, the tumor volumes of low-response tumors increased much faster than high-response tumors (Fig. 5D), and the survival curve revealed different outcomes for the two groups of tumors (Fig. 5E). This data implies that the median pO_2 value and hypoxic fraction of tumors acquired from CELI during the radiotherapy were highly relevant to understanding tumor response and outcomes in radiotherapy.

Discussion

The core hypothesis in this work was that there is a mismatch between the spatial resolution in imaging of tumor oxygenation possible with existing techniques, and the required resolution to adequately predict the response to radiation therapy. While most pre-clinical oxygen imaging is performed with PET using FAZA and FMISO tracers, and there are positive indications of its predictive value in small animal studies, this methodology is may have inaccuracy in the translation to human imaging given the differences between spatial resolution of microPET relative to whole body PET (25). Tissue pO_2 in tumors is known to be highly heterogeneous, and adequately quantifying the hypoxic fraction requires spatial resolution on the order of 100–200 microns. The ex vivo image analysis of pimonidazole stained sections in Fig 2 C, D & E was completed to determine the magnitude of changes expected. While imaging with pimonidazole has its own limitations, it was used in this work as a simple reference illustration to examine changes in the values of such parameters as hypoxic fractions obtained at different spatial resolutions. Given a tumor that is near 30% hypoxic, spatial resolutions near 500 microns or better were needed to estimate accurate the hypoxic fraction, that is within 10% of the value obtained at high resolution. However, as the sampling resolution decreased, the hypoxic fraction decreased, such that at 3mm the hypoxic fraction was 50% of the true value. Given that the hypoxic fraction is the parameter that likely best predicts radiation response or resistance, spatial resolutions of at least 500 microns may be needed to determine it accurately.

In vivo imaging of pO_2 was completed with CELI as shown in Fig 3. This approach was used to test our observations of dependencies coupled to imaging with different resolution. As shown in Fig 3E, the estimates of the median pO_2 increased slightly from 12 to 13 mmHg when the sampling resolution changed from 200 microns to 3mm, whereas in Fig 3F the hypoxic fraction decreased from 38% down to 10% at the same time. This suggests that estimation of the hypoxic fraction is more sensitive to spatial resolution changes versus a measure of median pO_2. As such, imaging at low spatial resolution might be sufficient for estimation of the tumor median pO_2, however the hypoxic fraction might be insufficiently sampled by most low-resolution imaging methods.

The question of which parameter provides the best metric for prediction of the tumor response to radiation was examined in the study carried out in two tumor lines: the MDA-MB-231 line, which is known to respond to radiation, and the FaDu line, which is known to be more resistant. In Fig 4C and D, the changes between days 1 and 5 of hypofractionated therapy were assessed for median pO_2 and hypoxic fraction, respectively. The observation that MDA-MB-231 pO_2 changes were significant was interesting, although the magnitude of the change was less than +2 mmHg in all cases. In comparison, the change in the hypoxic

fraction was only significant at high spatial resolution with changes in the range of −5% from the baseline of 40% hypoxic fraction. This supports the hypothesis here that the hypoxic fraction might be a more complete measure of radiation resistance, and have a higher dynamic range from which to sample changes.

The ability to predict the radiation response by pO_2 imaging is illustrated in Fig 5, where the imaged cohort was divided into the high and low responders of a single cluster of MDA-MB-231 tumors. Even though these were all the mice of same phenotype and having the same tumor cells, there was a range of responses to radiation, and the differences provided marker of the predictive value of spatially averaged pO_2 value *vs* that of hypoxic fraction. The most important conclusion is that when the imaging resolution changed from 200 microns to 3mm, the median pO_2 increased slightly, while the hypoxic fraction decreased significantly. The high spatial resolution was required to see significant changes between the two groups of animals, supporting our conclusion that high-resolution sampling of oxygen heterogeneity helps to predict the response to hypofractionated treatment.

In summary, this work used high-resolution pO_2 imaging of tumors to evaluate tumor hypoxia markers at the time of the radiation dose delivery. The influence of spatial resolution on the derived measures of hypoxia, such as median pO_2 and hypoxic fraction, reveal that the quantification accuracy can be significantly affected by the spatial resolution of imaging. Sub-millimeter spatial resolution imaging appears to be needed to obtain accurate information on tumor hypoxic fraction, and measures of median pO_2 seem to be less affected by the spatial resolution. However, when it comes to using oxygen measures as a metric of response to radiation, there is indication that the hypoxic fraction may be a viable tool to estimate response versus non-response.

Materials and Methods

Oxyphor PtG4.

The oxygen probe used in this study was Oxyphor PtG4 (SI Appendix, Fig. S1A) (32, 33, 38, 39). The molecular weight of Oxyphor PtG4 is ~35 kDa, and the approximate diameter of the molecule in an aqueous solution is ~5 nm. Therefore, Oxyphor PtG4 can easily diffuse into the tumor interstitial space from the leaky vasculature: a phenomenon known as enhanced permeability and retention (EPR) effect. The phosphorescence intensity and lifetime of Oxyphor PtG4 are strongly dependent on oxygen levels (SI Appendix, Fig. S1E and F). The response of the phosphorescence to oxygen was calibrated as described previously [refs 20, 21] as well as in the CELI setup [22] (SI Appendix, Fig. S1G). Oxyphor PtG4 was shown to be stable under high irradiation dose of 60Gy with 6 MV X-ray (SI Appendix, Fig. S1H).

Setup for CELI.

As shown in Fig.1A, the light source of CELI is Cherenkov light generated in tissues induced by a linear accelerator (Varian Linac 2100CD, Varian Medical System), at the Norris Cotton Cancer Center, Dartmouth-Hitchcock Medical Center. For radiotherapy, 6MV X-ray radiation delivered from the Linac with a beam size adjusted to cover the entire tumor

for treatment purpose. The CELI imaging system was previously reported. In brief, a time-gated intensified CCD camera (ICCD, PI-MAX4 1024i, Princeton Instruments) coupled with a commercial lens (Canon EF 135mmf/2L USM) was used as the detector. To shield the MV X-ray, the camera was put in a homemade lead box about 2 meters away from the imaging field. A band pass filter with center wavelength of 750 nm and spectral bandwidth of 100 nm was used to collect phosphorescence from Oxyphor PtG4. The time-gated ICCD camera was synchronized with the radiation pulse, which was ~3.25 μs long delivered at 360 Hz repetition rate from the Linac. Four CELI images were acquired with the delay times of 5 μs, 10 μs, 20 μs, and 30 μs to fit the lifetime image. To accumulate high enough phosphorescence signals, the intensifier gain was set to the maximum of 100, and 360 repeat cycles were integrated with 200 μs gate width in each cycle. The Linac room was kept dark during the acquisition to minimize stray light.

Animal imaging.

All animals were cared for and handled in accordance with National Institutes of Health Guidelines for the care and use of experimental animals and study protocol has been approved by the Dartmouth Institutional Animal Care and Use Committee (IACUC). Nude female mice at age of 6 weeks (Charles River Labs, Wilmington, MA) were injected with either 10^6 MDA-MB 231 cells or 10^6 Fadu cells, under the skin on the flank. Mice were housed in the institutional animal facility, fed standard laboratory diet and monitored daily. After approximately 2 weeks of growth, animals were chosen for imaging when their tumor diameter was approximately 8 mm in size. Oxyphor PtG4 was intravenously injected in the tail vein with 200μL at 200μM, at 24 h before CELI. During the imaging sessions the mice were under general anesthesia of inhaled isofluorane at 1.5%, in flowing air via nose cone during all treatment and imaging procedures.

Tumor cell lines.

The human breast cancer cell line MDA-MB-231 and human head neck cancer cell line Fadu cells were purchased directly from American Type Culture Collection (ATCC, Manassas Virginia), and they are not listed in the ICLAC database of cross-contaminated or misidentified cell lines. Cells were grown in culture media in an incubator at 37 °C in MEM with 10% (v/v) fetal bovine serum (FBS) and 1% penicillin streptomycin. When ready for use, cells were trypsonized, counted, spun down into a slurry, and used for inoculation into animals.

Pimonidazole stained tumor sections.

To obtain accurate hypoxia distributions at the micrometer scale in tumor tissue, MDA-MB-231tumors were stained with the hypoxia marker pimonidazole. The pimonidazole was injected in vivo in saline at a dosage of 1.5mg/mouse, at 1 hr prior to sacrifice, using animals with tumors grown for two weeks to a volume of 200–300 mm^3. After excision, the tumors were fixed by formalin and embedded in paraffin. For each tumor, 20–30 sections (10 μm thick) were cut at different depths. Staining of pimonidazole was done in each section by incubation with rabbit anti-pimonidazole antibody (Hypoxyprobe Inc., Burlington MA) diluted 1:1000 in primary antibody diluent for 30 mins at 37°C according to the provided protocol. The concentration of anti-pimonidazole antibody was titrated to achieve high

dynamic in staining intensity across the tumors, with minimal negative control stain. The second incubation step was with donkey-anti-rabbit Alexa488 (Molecular Probes, Leiden Netherlands) diluted 1:600 in PBS. For negative control pimonidazole staining, samples of tissue with no pimonidazole, anti-pimonidazole antibody, and a second antibody were also developed and quantified. Pimonidazole stained slides were imaged with a Vectra 3 automated quantitative pathology imaging system (PerkinElmer, Inc. Waltham MA).

Supplementary Material

Refer to Web version on PubMed Central for supplementary material.

Acknowledgments

This work was funded by the grants R01 EB024498 (BWP), U24 EB028941 and R21 EB027397 (SAV) from the National Institutes of Health as well as by shared irradiation resources from the Norris Cotton Cancer Center (funded by P30 CA023108 (BWP).

References

1. Brown JM & Giaccia AJ (1998) The unique physiology of solid tumors: opportunities (and problems) for cancer therapy. Cancer research 58(7):1408–1416. [PubMed: 9537241]
2. Moeller BJ, Richardson RA, & Dewhirst MW (2007) Hypoxia and radiotherapy: opportunities for improved outcomes in cancer treatment. Cancer and Metastasis Reviews 26(2):241–248. [PubMed: 17440683]
3. Moulder JE & Rockwell S (1987) Tumor hypoxia: its impact on cancer therapy. Cancer and metastasis reviews 5(4):313–341. [PubMed: 3552280]
4. Bhandari V, et al. (2019) Molecular landmarks of tumor hypoxia across cancer types. Nature genetics 51(2):308–318. [PubMed: 30643250]
5. Harrison LB, Chadha M, Hill RJ, Hu K, & Shasha D (2002) Impact of tumor hypoxia and anemia on radiation therapy outcomes. The oncologist 7(6):492–508. [PubMed: 12490737]
6. Vaupel P & Mayer A (2007) Hypoxia in cancer: significance and impact on clinical outcome. Cancer and Metastasis Reviews 26(2):225–239. [PubMed: 17440684]
7. Benej M, et al. (2018) Papaverine and its derivatives radiosensitize solid tumors by inhibiting mitochondrial metabolism. Proceedings of the National Academy of Sciences 115(42):10756–10761.
8. Bettegowda C, et al. (2003) Overcoming the hypoxic barrier to radiation therapy with anaerobic bacteria. Proceedings of the National Academy of Sciences 100(25):15083–15088.
9. Horsman MR, Mortensen LS, Petersen JB, Busk M, & Overgaard J (2012) Imaging hypoxia to improve radiotherapy outcome. Nature reviews Clinical oncology 9(12):674.
10. Rajendran J, et al. (2006) Hypoxia imaging-directed radiation treatment planning. European journal of nuclear medicine and molecular imaging 33(1):44–53. [PubMed: 16763816]
11. Bussink J, Kaanders JH, Van Der Graaf WT, & Oyen WJ (2011) PET–CT for radiotherapy treatment planning and response monitoring in solid tumors. Nature Reviews Clinical Oncology 8(4):233.
12. Brown JM & Wilson WR (2004) Exploiting tumour hypoxia in cancer treatment. Nature Reviews Cancer 4(6):437–447. [PubMed: 15170446]
13. Nozue M, et al. (1997) Interlaboratory variation in oxygen tension measurement by Eppendorf “Histograph” and comparison with hypoxic marker. Journal of surgical oncology 66(1):30–38. [PubMed: 9290690]
14. Nordsmark M, et al. (2006) The prognostic value of pimonidazole and tumour pO2 in human cervix carcinomas after radiation therapy: a prospective international multi-center study. Radiotherapy and Oncology 80(2):123–131. [PubMed: 16890316]

15. Hicks RJ, et al. (2005) Utility of FMISO PET in advanced head and neck cancer treated with chemoradiation incorporating a hypoxia-targeting chemotherapy agent. European journal of nuclear medicine and molecular imaging 32(12):1384–1391. [PubMed: 16133382]
16. Thorwarth D, Eschmann SM, Paulsen F, & Alber M (2005) A kinetic model for dynamic [18F]-Fmiso PET data to analyse tumour hypoxia. Physics in Medicine & Biology 50(10):2209. [PubMed: 15876662]
17. Halmos GB, et al. (2014) Head and neck tumor hypoxia imaging by 18F-fluoroazomycin-arabinoside (18F-FAZA)-PET: a review. Clinical nuclear medicine 39(1):44–48. [PubMed: 24152663]
18. Busk M, et al. (2008) Imaging hypoxia in xenografted and murine tumors with 18F-fluoroazomycin arabinoside: a comparative study involving microPET, autoradiography, PO2-polarography, and fluorescence microscopy. International Journal of Radiation Oncology* Biology* Physics 70(4):1202–1212.
19. Piert M, et al. (2005) Hypoxia-specific tumor imaging with 18F-fluoroazomycin arabinoside. Journal of Nuclear Medicine 46(1):106–113. [PubMed: 15632040]
20. Di Perri D, et al. (2017) Evolution of [18F] fluorodeoxyglucose and [18F] fluoroazomycin arabinoside PET uptake distributions in lung tumours during radiation therapy. Acta Oncologica 56(4):516–524. [PubMed: 28358668]
21. Grosu A-L, et al. (2007) Hypoxia imaging with FAZA-PET and theoretical considerations with regard to dose painting for individualization of radiotherapy in patients with head and neck cancer. International Journal of Radiation Oncology* Biology* Physics 69(2):541–551.
22. Schuetz M, et al. (2010) Evaluating repetitive 18F-fluoroazomycin-arabinoside (18FAZA) PET in the setting of MRI guided adaptive radiotherapy in cervical cancer. Acta Oncologica 49(7):941–947. [PubMed: 20831481]
23. Busk M, Horsman MR, & Overgaard J (2008) Resolution in PET hypoxia imaging: voxel size matters. Acta Oncologica 47(7):1201–1210. [PubMed: 18661432]
24. Grimes DR, Warren DR, & Warren S (2017) Hypoxia imaging and radiotherapy: bridging the resolution gap. The British journal of radiology 90(1076):20160939. [PubMed: 28540739]
25. Phelps ME, Chatziioannou A, Cherry S, & Gambhir S (2002) Molecular imaging of biological processes from microPET in mice to PET in patients. Proceedings IEEE International Symposium on Biomedical Imaging, (IEEE), pp 1–9.
26. Vaupel P, Höckel M, & Mayer A (2007) Detection and characterization of tumor hypoxia using pO2 histography. Antioxidants & redox signaling 9(8):1221–1236. [PubMed: 17536958]
27. Vanderkooi JM, Maniara G, Green TJ, & Wilson DF (1987) An optical method for measurement of dioxygen concentration based upon quenching of phosphorescence. Journal of Biological Chemistry 262(12):5476–5482.
28. Rumsey WL, Vanderkooi JM, & Wilson DF (1988) Imaging of phosphorescence: a novel method for measuring oxygen distribution in perfused tissue. Science 241(4873):1649–1651. [PubMed: 3420417]
29. Bruza P, et al. (2016) Light sheet luminescence imaging with Cherenkov excitation in thick scattering media. Opt Lett 41(13):2986–2989. [PubMed: 27367082]
30. Jia MJ, et al. (2019) Cherenkov-excited luminescence scanned imaging using scanned beam differencing and iterative deconvolution in dynamic plan radiation delivery in a human breast phantom geometry.
31. Zhang R, et al. (2015) Cherenkov-excited luminescence scanned imaging. Opt Lett 40(5):827–830. [PubMed: 25723443]
32. Esipova TV, et al. (2011) Two new “protected” oxyphors for biological oximetry: properties and application in tumor imaging. 83(22):8756–8765.
33. Lebedev AY, et al. (2009) Dendritic phosphorescent probes for oxygen imaging in biological systems. 1(6):1292–1304.
34. Cao X, et al. (2020) Tissue pO 2 distributions in xenograft tumors dynamically imaged by Cherenkov-excited phosphorescence during fractionated radiation therapy. Nature Communications 11(1):1–9.

35. Zhang RX, et al. (2013) Oxygen tomography by Cerenkov-excited phosphorescence during external beam irradiation. J Biomed Opt 18(5):050503.

36. Pogue BW, et al. (2018) Maps of in vivo oxygen pressure with submillimetre resolution and nanomolar sensitivity enabled by Cherenkov-excited luminescence scanned imaging. Nat Biomed Eng 2(4):254–264. [PubMed: 30899599]

37. Holt RW, et al. (2014) Cherenkov excited phosphorescence-based pO2 estimation during multi-beam radiation therapy: phantom and simulation studies. Physics in Medicine & Biology 59(18):5317. [PubMed: 25146556]

38. Sullender CT, et al. (2018) Imaging of cortical oxygen tension and blood flow following targeted photothrombotic stroke. Neurophotonics 5(3):035003. [PubMed: 30137881]

39. Christodoulou C, et al. (2020) Live-animal imaging of native haematopoietic stem and progenitor cells. Nature 578(7794):278–283. [PubMed: 32025033]

Statement of Significance

Accurate evaluation of radiobiologically relevant levels of hypoxia in solid tumors is important for understanding radiotherapy failures and planning dose boost to these areas. Positron emission tomography (PET) of hypoxia with FAZA or FMISO probes is used in clinical radiotherapy treatment studies today, but this method has approximately 3 mm spatial resolution and provides a spatially averaged estimate of the average oxygenation level. However, tumor oxygen levels are heterogeneous on a spatial scale of just hundreds of microns, and imaging with low spatial resolution can lead to inaccurate quantification of hypoxic fraction and subsequent underestimation of the effect on radiation resistance. In the present work, imaging of pO_2 by oxygen-dependent quenching of phosphorescence was used to sample tumor oxygenation with submillimeter resolution, to examine which parameters were relevant for adequate prediction of the radiation response. Our results demonstrate that the most relevant parameter is hypoxic fraction, which is strongly dependent upon the spatial resolution of the imaging method.

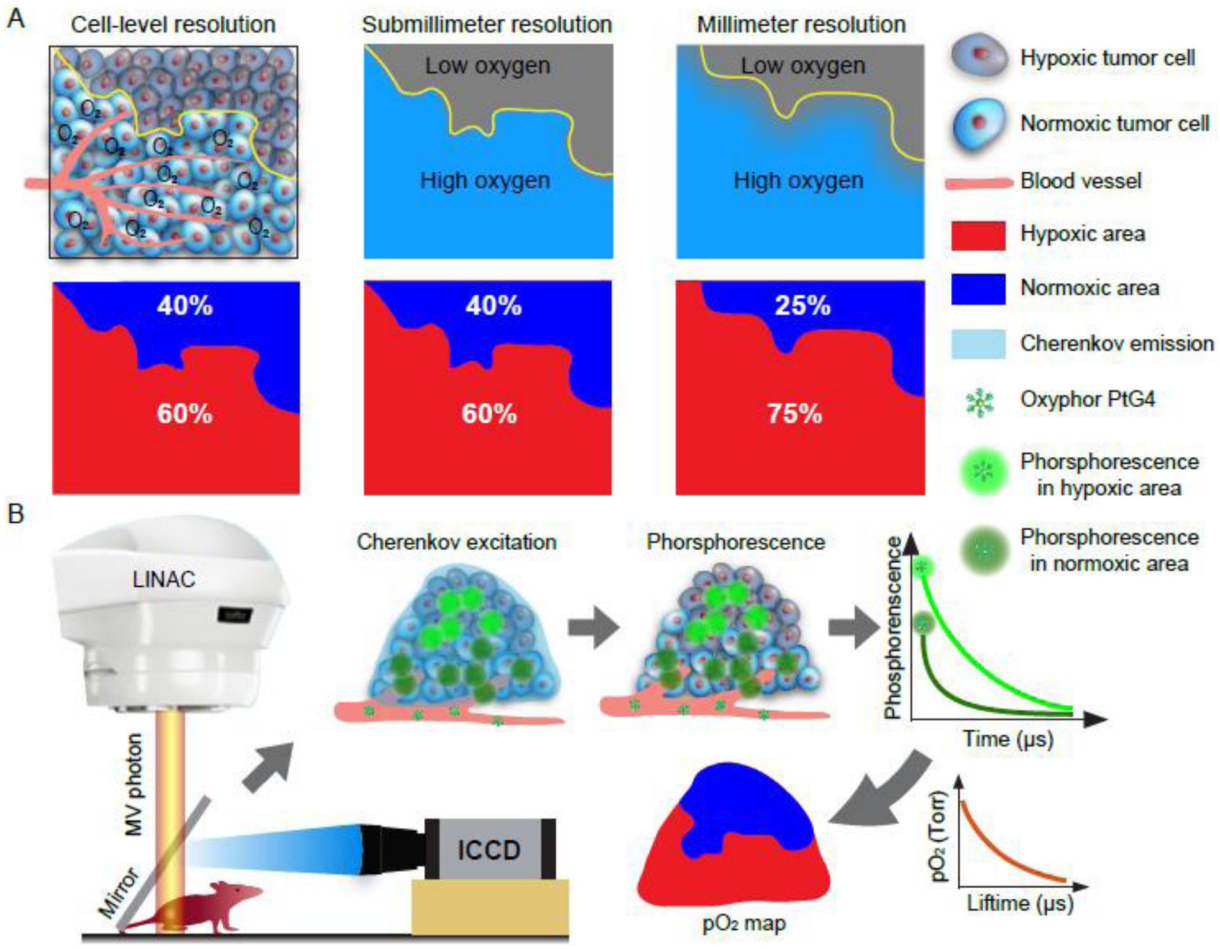

Fig. 1.

(A) Schematic diagram shows the influence of spatial resolution on the estimation of the hypoxic fraction. (B) Workflow diagram of *in vivo* pO_2 imaging based on Cherenkov Excited Luminescence Imaging (CELI).

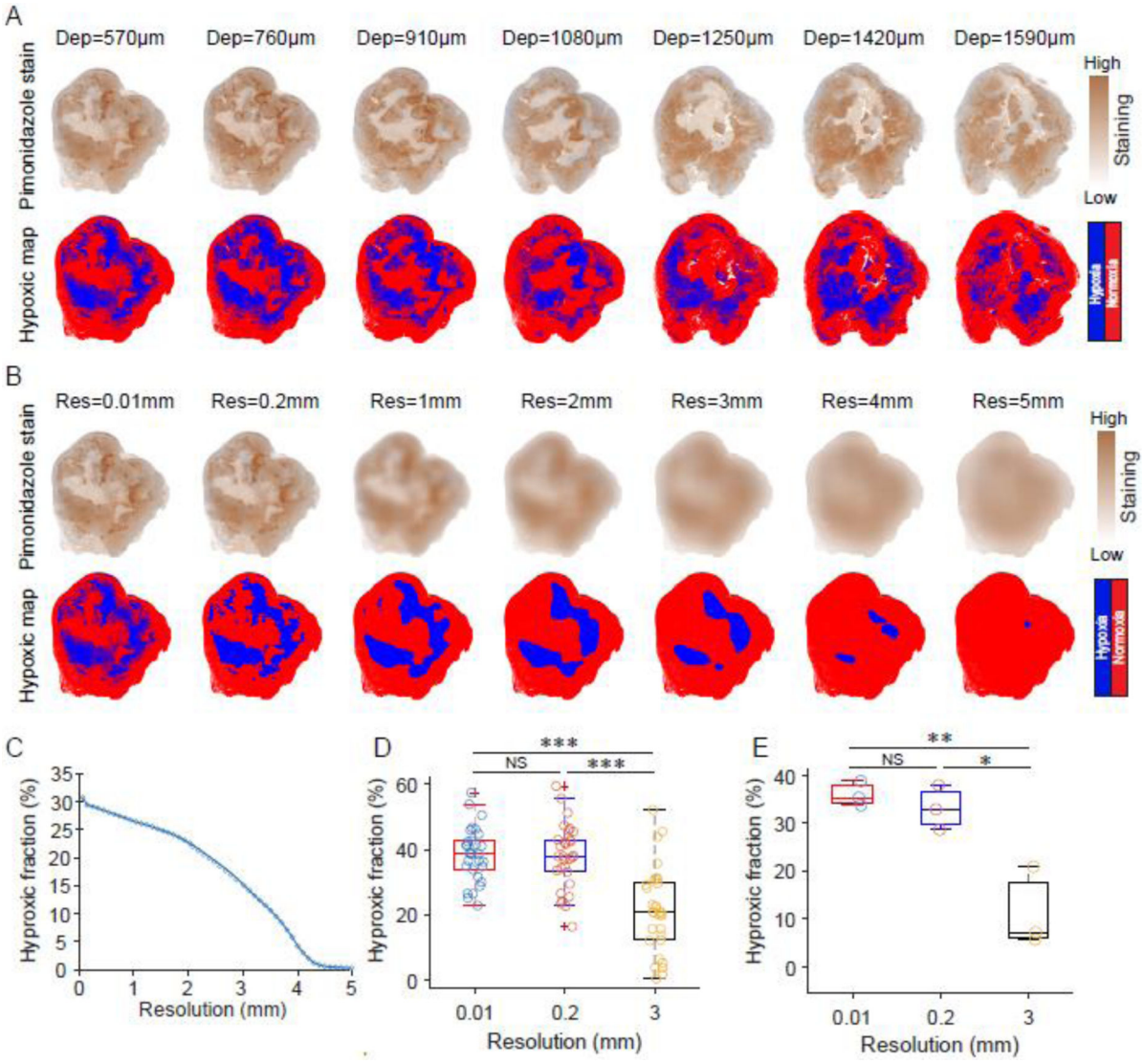

Fig. 2.

Immunohistochemistry image assessment of estimated tumor hypoxia relative to image spatial resolution. (A) Pimonidazole sections at different depths. The hypoxic map was obtained by segmentation of the pimonidazole stanning image with a cut-off threshold ratio of 1.5 compared to normal tissues. (B) The influence of resolution on the quantification of hypoxic fraction. The pimonidazole staining was spatially smoothed to illustrate what is achieved at different spatial resolutions and the corresponding hypoxic areas segmented. (C) The resulting hypoxic fractions estimated versus spatial resolution. The hypoxic fraction was estimated by the ratio of hypoxic area to the whole area of the section based on the segmented maps. (D) The hypoxic fractions of 27 sections for a tumor obtained with different spatial resolutions. (E) The hypoxic fractions of three tumors were obtained with different spatial resolutions. The hypoxic fraction of a tumor was the average value of hypoxic fractions of all sections cut for the tumor. A paired t-test was used for statistical analysis with significance levels denoted by: *P < 0.01, **P < 0.0001, **P < 0.000001, and

NS denoting no significance. Boxplots shows median and interquartile range, whiskers indicate the range.

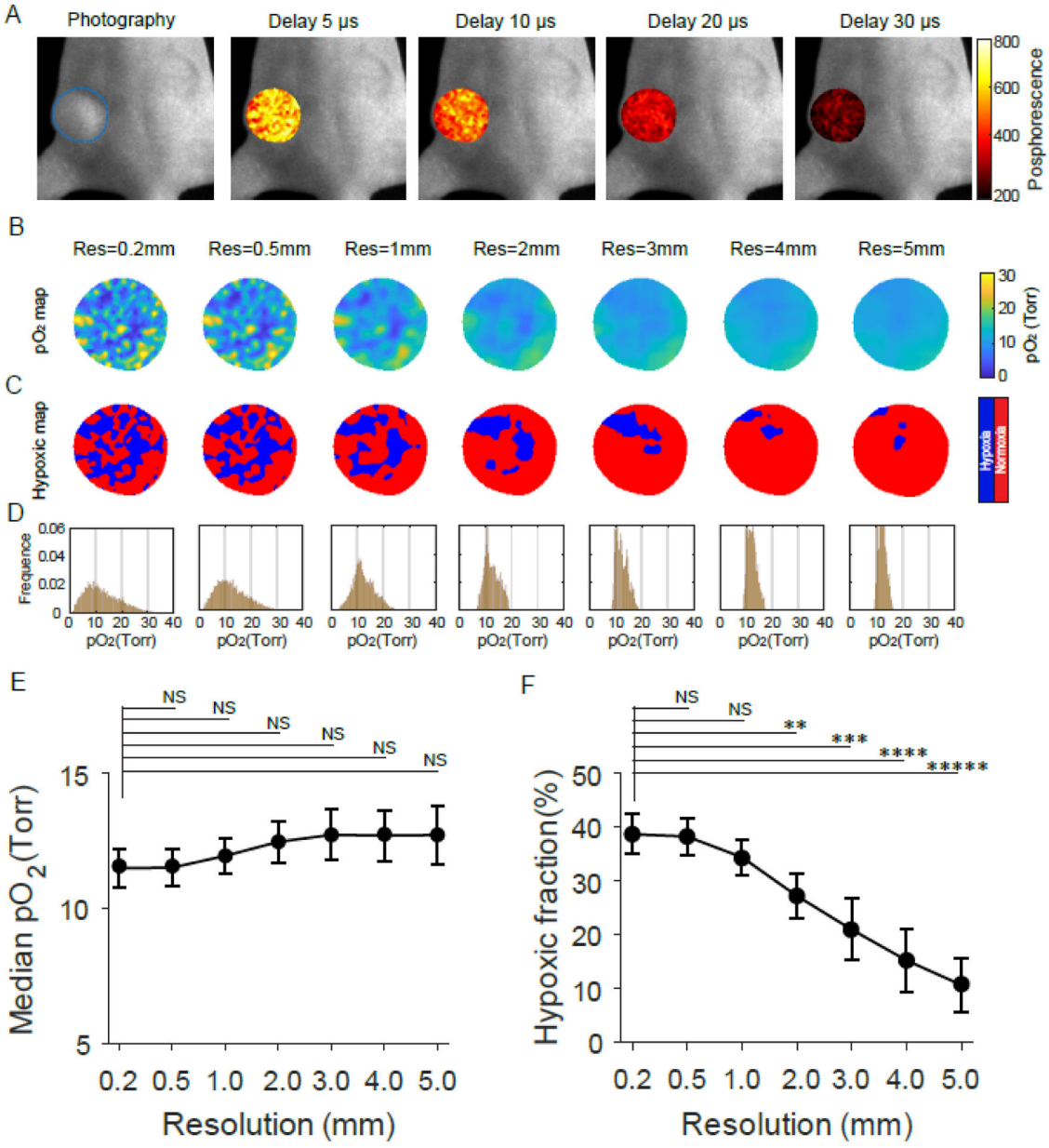

Fig. 3.

In vivo assessment of tumor oxygen parameters based on pO_2 imaging at different spatial resolutions. (A) Phosphorescence intensity images acquired at different time delays relative to the radiation pulse during radiotherapy. (B to D) The pO_2 maps (B), Hypoxic maps (C), and pO2 histograms (D) of the tumor for different spatial resolutions. (E and F) Median pO_2 values (E) and hypoxic fractions (F) of tumors changed with the spatial resolutions. Data in (E) and (F) are means ± std (n = 5). A paired t-test was used for statistical analysis with significance denoted by: *P < 0.01, ***P < 0.00001, ****P < 0.000001, and NS meaning no significance.

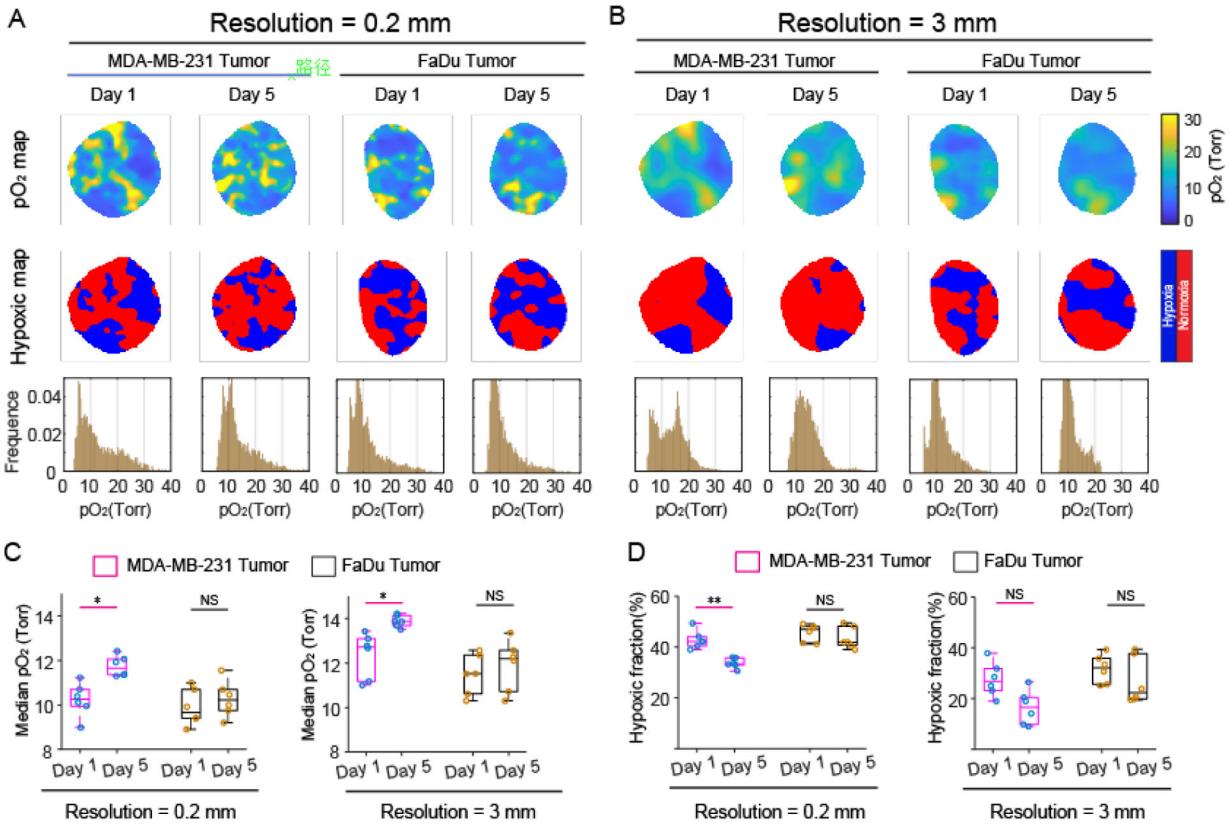

Fig. 4.

Assessment of oxygen parameter changes during hypofractionated radiotherapy in MDA-MB-231 and FaDu tumors with two spatial resolutions. (A and B) The pO_2 maps hypoxic maps, and pO_2 histograms for 0.2 mm (A), and 3 mm (B) spatial resolutions. (C and D) Estimated median pO_2 values and (C and D) hypoxic fractions for 0.2mm (left) and 3mm (right) resolutions. A paired t-test was used for statistical analysis (n = 6). *P < 0.01, **P < 0.0001. Boxplot shows median and interquartile range, whiskers indicate the range.

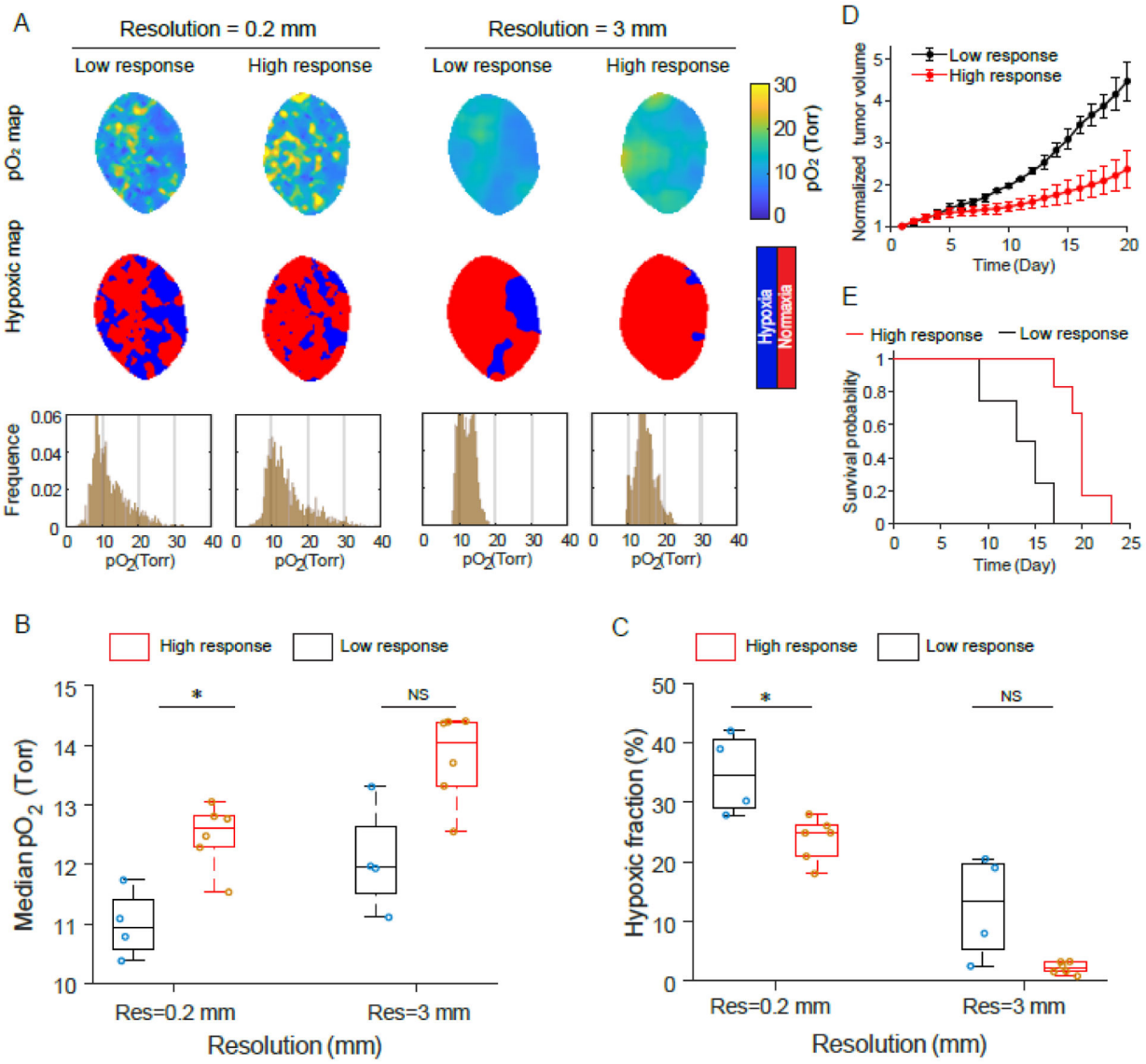

Fig. 5.

Testing predictive value of in vivo pO_2 imaging in initial radiotherapy fraction for the final tumor outcome with two spatial resolutions. (A and B) The pO_2 maps, hypoxic maps and pO_2 histograms for high-response (A) and low-response (B) tumors to radiotherapy. (C and D) Tumor volume growth (C) and survival curve (D) for high-response and low-response tumors. (E and F) Median pO2 values (E) and hypoxic fractions (F) for high-response and low-response tumors with 0.2 mm and 3 mm resolutions. Two-sample t-test was used for statistical analysis. *P < 0.01, ****P < 0.000001. Boxplots show median and interquartile range, whiskers indicate the range.